Carbon 181 (2021) 79–86

Contents lists available at ScienceDirect

Carbon

journal homepage: www.elsevier.com/locate/carbon

Surface zeta potential and diamond growth on gallium oxide single crystal

Soumen Mandal [a, *], Karsten Arts [b], Harm C.M. Knoops [b, c], Jerome A. Cuenca [a], Georgina M. Klemencic [a], Oliver A. Williams [a, **]

[a] School of Physics and Astronomy, Cardiff University, Cardiff, UK
[b] Eindhoven University of Technology, 5612 AZ, Eindhoven, the Netherlands
[c] Oxford Instruments Plasma Technology, North End, Yatton, Bristol, BS49 4AP, UK

ARTICLE INFO

Article history:
Received 2 April 2021
Received in revised form
27 April 2021
Accepted 30 April 2021
Available online 17 May 2021

Keywords:
Diamond
Zeta potential
Gallium oxide

ABSTRACT

In this work a strategy to grow diamond on β-Ga_2O_3 has been presented. The ζ-potential of the β-Ga_2O_3 substrate was measured and it was found to be negative with an isoelectric point at pH ~ 4.6. The substrates were seeded with mono-dispersed diamond solution for growth of diamond. The seeded substrates were etched when exposed to diamond growth plasma and globules of gallium could be seen on the surface. To overcome problem ~100 nm of SiO_2 and Al_2O_3 were deposited using atomic layer deposition. The nanodiamond seeded SiO_2 layer was effective in protecting the β-Ga_2O_3 substrate and thin diamond layers could be grown. In contrast Al_2O_3 layers were damaged when exposed to diamond growth plasma. The thin diamond layers were characterised with scanning electron microscopy and Raman spectroscopy. Raman spectroscopy revealed the diamond layer to be under compressive stress of 1.3–2.8 GPa.

1. Introduction

In the semiconducting industry silicon is the most widely used material. The band gap of Si is well suited for tailoring the conductivity from semi-insulating to conducting. It also allows for the formation of both n-type and p-type material. As a result the application landscape of Si in the semiconducting industry is vast. Nonetheless, there are areas of applications in which Si as a material is not well suited. For example, many high temperature applications are dependent on the breakdown electric field strength (E_{br}), which has a strong correlation with the bandgap. To overcome the limitations of silicon in high temperature applications, many wide bandgap (2.0 eV $\leq E_g \leq$ 7.0eV) [1] compound semiconductors like SiC (E_g = 2.4 – 3.2 eV) [1] and GaN(E_g = 3.39 eV) [2] have been developed. Even as wide band gap electronics based on SiC and GaN are maturing, newer materials with wider band gaps ($E_g >$ 3.4 eV) are appearing on the horizon. One of the ways to compare different semiconductors is through figures of merit. For low frequency operations, the Baliga figure of merit(BFM) [3] is widely used and for high frequency operations Johnsons figure of merit(JFM) [4] is widely accepted. Based on BFM of different wide band gap materials, β-Ga_2O_3, AlN, diamond and c-BN are some of the materials that are considered superior to GaN and SiC [5]. Of these four materials, β-Ga_2O_3 has attracted a lot of attention in recent times [5–10], mostly due to availability of large substrates. These large substrates are grown by several melt growth methods like float zone [11,12], Czochralski [13,14], Bridgman [15,16] and edge-defined film-fed growth (EFG) [6,17,18].

While the study in growth of large substrates is an on-going topic, researchers have already demonstrated devices made from gallium oxide [19–27]. The demonstrated devices point towards promising advantages in gallium oxide over traditional wide band gap semiconductors like SiC and GaN. However, as with most high power devices, thermal management in gallium oxide devices, with its low thermal conductivity (10–30 W/mK) [28], is a major bottle neck in the development of technology based on this material [9]. It is a well known fact that higher operation temperature in high power devices can lead to significantly lower lifetimes [29,30]. One way researchers have overcome this problem is by exfoliating gallium oxide [26,27,31] or by growing gallium oxide on single crystal diamond(thermal conductivity ~ 2000 W/mK) substrates

* Corresponding author.
** Corresponding author.
E-mail addresses: mandals2@cardiff.ac.uk (S. Mandal), williamso@cardiff.ac.uk (O.A. Williams).

https://doi.org/10.1016/j.carbon.2021.04.100

[32]. Another approach that has been recently demonstrated is low temperature bonding of single crystal diamond on β-Ga_2O_3 [33]. The major drawback in all these approaches is the small area of the resulting heterostructure for device fabrication. Availability of large area single crystal is currently very limited [34] or very expensive. An alternative approach can be direct bonding of large β-Ga_2O_3 crystals to chemical mechanical polished [35–37] flat polycrystalline diamond films. This technique is also not straightforward and will involve non-trivial sample surface preparations. A solution to the thermal management problem can be to grow a thick diamond layer on β-Ga_2O_3 single crystal similar to what we have shown in the past on AlN thin films [38]. Another potential application for direct diamond growth can be formation of ultrawide-bandgap p-n heterojunction. In this case thin layers of boron doped diamond can be directly grown on gallium oxide substrates. Such devices have already been demonstrated by Kim et al. [27] using single crustal diamond and exfoliated gallium oxide.

The growth of diamond on non-diamond substrates is not trivial. The surface energy of diamond is ~ 6 J/m^2[39]. In comparison the surface energy of silicon, which is most commonly used substrate, is ~ 1.5 J/m^2 [40]. Due to this large surface energy difference heteroepitaxial growth of diamond is not possible [41,42] and results in only isolated diamond islands. On silicon the density of such islands are of the order of $10^4 - 10^5 cm^{-2}$. With a surface energy of ~ 1 J/m^2 [43] for β-Ga_2O_3, similar island formations are expected for heteroepitaxial growth. Hence, a seeding/nucleation technique is essential for growth of diamond films on gallium oxide surfaces. An additional issue with growth of diamond on non-diamond substrates using typical CVD approaches is the exposure of the sample to chemically reactive H_2 plasma. For example, there are well-known challenges for depositing diamond on GaN [38]. Additionally, H_2 plasmas are also known to cause surface damage to β-Ga_2O_3[44]. In this work, growth of diamond on β-Ga_2O_3 substrates has been demonstrated. The ζ - potential of the substrates have been measured to determine the best seeding solution. It was found that the substrates disintegrate when exposed to plasma during diamond growth leaving behind globules of gallium. To overcome this, a thin layer of SiO_2 and Al_2O_3 was deposited as a buffer layer. The ζ-potential of the buffer layers were also measured. Thin diamond films were grown (250 nm) and characterised using scanning electron microscopy. Also, the film stresses were characterised using Raman spectroscopy. For deposition of thick diamond layers alternative strategies will have to be designed to manage the stress at the interface, which will be the basis of further studies.

2. Experiment

When a solid is immersed in a liquid it acquires a surface charge which is compensated by ions of opposite charge or counterions that are loosely bound to the surface. The surface charge is formed due to adsorbed ions on the surface of solid and that forms the first layer. The counterions are then attracted towards the surface due to Coulomb attraction and are part of a second layer called diffuse layer. The first layer is immobile with respect to solid. The surface charges also generate a potential which decays with distance from the solid surface. ζ-potential is defined as the potential at the boundary of the immobile and mobile liquid with respect to rest of the liquid. For measuring ζ-potential it is essential to measure the charge on the counterions. If a channel is formed between two solid surfaces and an electrolyte is passed through the channel, the counterions experience a shearing force and move along with the electrolyte [45]. As a result a charge separation is formed between the inlet and outlet of the channel. This leads to formation of an electric potential known as streaming potential. First suggested by Van Wagenen et al. [45], it has been used for determination of ζ-potential of variety of surfaces [38,46–52]. The Helmholtz-Smoluchowski equation gives a relation between ζ-potential and streaming current/potential [53]. By measuring the change in streaming current/potential as a function of electrolyte pressure the ζ-potential can be determined. The ζ-potential of β-Ga_2O_3, SiO_2 and Al_2O_3 coated β-Ga_2O_3, sapphire and quartz were measured using Surpass^{TM} 3 electrokinetic analyzer. In the present work the channel width was kept between 90 and 110 μm. The electrolyte was 10^{-3} M solution of KCl in DI water with electrolyte pressure varying between 200 and 600 mbar. The pH of the electrolyte was varied by addition of 0.1 M NaOH and 0.1 M HCl solution with the inbuilt titrator in Surpass^{TM} 3.

The ~100 nm SiO_2 and Al_2O_3 layers were grown by atomic layer deposition (ALD), using an Oxford Instruments FlexAL reactor [54]. Both layers were grown using 1100 ALD cycles and a table temperature setpoint of 300 °C. The SiO_2 layer was grown using $SiH_2(NEt_2)_2$ (bis(diethylamino)silane) as precursor and O_2 plasma as coreactant, where the O_2 plasma was generated by an inductively coupled plasma source. Purely thermally-driven ALD was employed for the growth of Al_2O_3, using $Al(CH_3)_3$ (trimethylaluminum) and H_2O. The thicknesses of the deposited SiO_2 and Al_2O_3 layers were measured by spectroscopic ellipsometry (SE), using a M–2000D Spectroscopic Ellipsometer of J.A. Woollam Co. The SE measurements were performed ex-situ on silicon substrates (Czochralski silicon (100) with ~1.6 nm native oxide) that were processed alongside the β-Ga_2O_3 substrates. A Cauchy dispersion model was used for fitting the SE data [55]. The film thicknesses were measured to be 89 nm for the SiO_2 layer and 111 nm for the Al_2O_3 layer. Moreover, the refractive indices of the films (at 632.8 nm) were measured as 1.45 for SiO_2 and 1.65 for Al_2O_3.

After ζ-potential measurements the substrates were seeded with mono-dispersed diamond solution. This seeding technique is known to create a seed density in excess of 10^{11} cm^{-2} and the details of the seeding process can be found here [41,42]. The seeded wafers were then introduced in a Carat Systems SDS6U microwave plasma chemical vapour deposition(MPCVD) systems. The growth was done in two steps, that is incubation and growth. The growth of diamond by MPCVD is essentially a complex process of growth and etching of all forms of carbon with non-diamond carbon surviving only in negligible quantities. The nanodiamond seeds used for seeding are typically 5 nm in size. As a result they have considerable surface to volume ratio resulting in large proportion of non-diamond carbon [41] at the surface which are easily etched in the plasma. The incubation step, lasting for 3–10 min, is used for fast growth of seeds so that they are not fully etched away during initial stages of growth. For the incubation step a gas mixture of 5% CH_4/H_2 and 50 torr chamber pressure with 3.7 kW microwave power was used. The incubation period was 5 min and the gas flow was maintained at 500 sccm. After the incubation period the gas mixture was modified to 3% CH_4/H_2. The total time for the growth was 40 min and the growth temperature was 630 °C as recorded by dual wavelength Williamson pyrometer. The substrate temperature was kept low to reduce the thermal stress created due to difference between the thermal expansion coefficients of diamond [56] and β-Ga_2O_3[57]. After growth the sample was slowly cooled in hydrogen plasma. The substrates, diamond layers and oxide coating were analysed using a Horiba LabRAM HR Evolution equipped with SynapsePlus Back-Illuminated Deep Depletion (BIDD) CCD. The spectroscope is equipped with three lasers having wavelengths of 473, 532 and 660 nm. Data from all three lasers have been included in this work. A Hitachi SU8200 series scanning electron microscope (SEM) operating at 10 kV and working distances between 9 and

11 mm was used for imaging the samples after growth. $(\bar{2}01)$ β-Ga_2O_3 substrates used in this work were commercially sourced from Tamura Corporation. The substrates were single side chemical mechanical polished. 10 × 10mm and 5 × 5mm pieces were cut from a 2" wafer for growth of diamond.

3. Results and discussion

3.1. Zeta potential measurement

The determination of the ζ-potential of a non-diamond substrate, which is directly related to surface charge, is essential for the determination of the type of seed solution needed for high seed density. It is possible to create diamond seed solution with positive or negative surface charge in water [41,42,58]. For high seed density seed solution with charged particles opposite to charges on substrate surface are essential. Fig. 1 shows the ζ-potential as a function of electrolyte pH for β-Ga_2O_3 along with potentials of ALD deposited SiO_2, Al_2O_3, quartz and sapphire. The ζ-potential of β-Ga_2O_3 is negative beyond the isoelectric point around pH ∼ 4.6. This is in contrast to gallium oxide nanoparticles which have an isoelectric point of pH∼9 [59]. However, ζ-potential of single crystal β-Ga_2O_3 plate is similar to the ζ-potential for Ga faced GaN [49] where as, N-face GaN has more negative ζ-potential. The higher negative ζ of N-faced GaN could be down to higher amounts of adsorbed oxygen on the surface. However, the main point of interest for seeding is around pH 6–7. In this range the ζ potential of β-Ga_2O_3 is negative with a value between −20 and −30mV. This means that for high seed density H-terminated diamond seed solution is needed [58]. The substrates were seeded by dipping in H-terminated nanodiamond solution. The seeded substrates were then exposed to H_2/CH_4 plasma for diamond growth. As soon as the substrates were exposed to the plasma, immediate damage to the β-Ga_2O_3 surface could be observed. On closer examination under SEM (see later in Fig. 2), globules of gallium metal was observed.

To overcome the damage to the substrate surface from the plasma, it was encapsulated with a dielectric coating. For the purpose of the current study, SiO_2 and Al_2O_3 were chosen. Thin layers

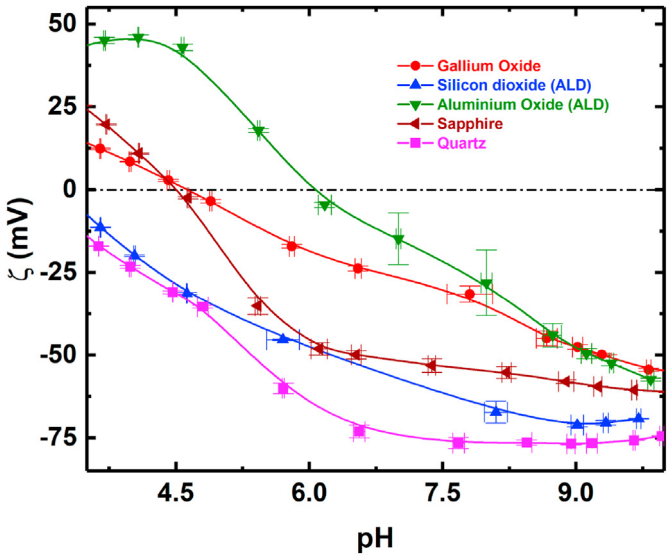

Fig. 1. Zeta potential vs pH for β-Ga_2O_3 crystal. The figure also show the zeta potential of deposited buffer layers namely, SiO_2 and Al_2O_3. The zeta potential of quartz and sapphire are shown for comparison as well. The solid lines are a guide to the eye. The dashed black line has been put to mark the isoelectric point. (A colour version of this figure can be viewed online.)

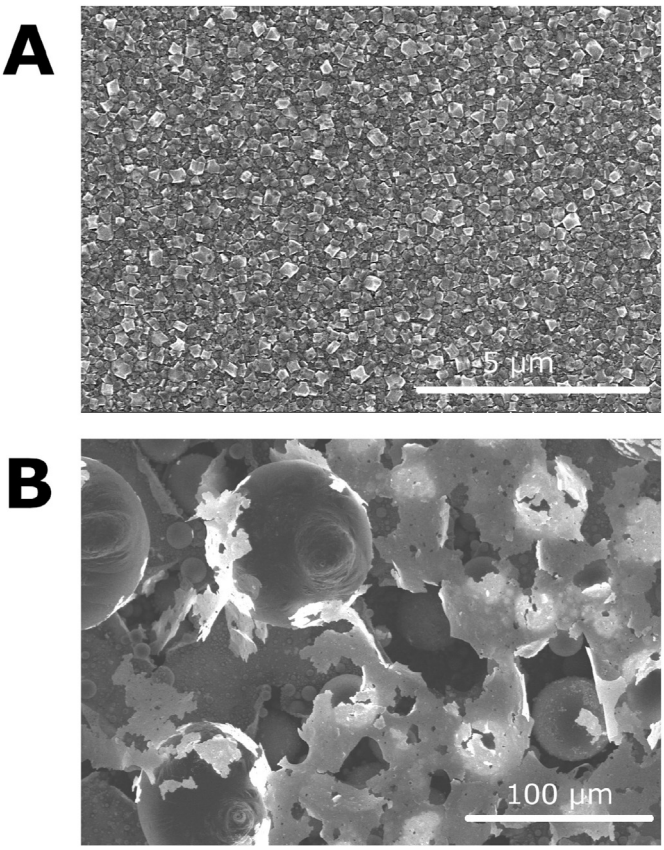

Fig. 2. A. Scanning electron microscope image of thin diamond film grown on SiO_2 coated β-Ga_2O_3. B. Image of the Al_2O_3 coated β-Ga_2O_3 surface after exposure to diamond growth condition. Tiny gallium globules along with flakes of Al_2O_3 can be clearly seen.

of the coatings were deposited with ALD. For measuring the zeta potential of the deposited coatings, quartz pieces were included during the deposition of the dielectrics on β-Ga_2O_3. The ζ potential of 100 nm ALD deposited dielectrics are shown in Fig. 1. For comparison ζ-potential of the quartz (SiO_2) and sapphire (Al_2O_3) are also shown. While SiO_2 has negative ζ-potential over the whole measurement range (pH ∼ 3–10), Al_2O_3 has isoelectric point at pH ∼ 6 and has negative ζ-potential beyond that point. In the case of SiO_2 the ζ-potential is not dependent on whether it is in the form of quartz, thin layer or nanoparticles [60]. In contrast, for Al_2O_3 it has a strong dependence on whether it is in the form of sapphire (isoelectric point pH ∼ 4.5), thin film (isoelectric point pH ∼ 6) or nanoparticles (isoelectric point pH ∼ 9) [61], which is similar to what is seen for gallium oxide. As before the substrates with dielectric encapsulation were seeded with H-terminated diamond seed solution. The seeded samples were exposed to diamond growth conditions. Thin diamond films could be grown on substrates encapsulated with SiO_2. The Al_2O_3 thin layer disintegrated on exposure to plasma and exposed the underlying β-Ga_2O_3 surface. This is probably due to large thermal mismatch between Al_2O_3 layer and β-Ga_2O_3. Alternatively, it is also possible that Al_2O_3 is easily etched [62] in CH_4/H_2 plasma while SiO_2 can act as a mask [63] in the same environment.

3.2. Scanning electron microscopy

Fig. 2A shows the scanning electron microscope images for diamond thin films grown on SiO_2 coated β-Ga_2O_3. A fully coalesced

film with grain sizes of the order of 250 nm can be clearly seen. Panel B in the image shows sample surface coated with Al_2O_3. The Al_2O_3 coating has completely disintegrated in the diamond growth plasma. Small flakes of Al_2O_3 can be clearly seen in the image. Once the Al_2O_3 layer disintegrates, the β-Ga_2O_3 surface is exposed to plasma and small gallium globules are formed. Such globules were also seen for samples that were not coated with a protective oxide.

3.3. Raman spectroscopy

In this section we will discuss the Raman spectra of β-Ga_2O_3, SiO_2 coated β-Ga_2O_3 and diamond grown on SiO_2 coated β-Ga_2O_3. A detailed comparison between β-Ga_2O_3 and SiO_2 coated β-Ga_2O_3 will be done to investigate the effects of the SiO_2 layer on the Raman modes of β-Ga_2O_3. β-Ga_2O_3 unit cell has 30 phonon modes [64,65], of these only 27 are optically active. Amongst the optically active modes 15 are Raman active which have A_g and B_g symmetry. Since only the modes with A_g and B_g symmetry are Raman active in β-Ga_2O_3, $Ag^{(1)}$ will be denoted simply as A1, where $Ag^{(1)}$ has a spectral position at 111 cm^{-1} according to Kranert et al. [65]. The rest of the Raman modes will follow similar convention throughout this article. The Raman spectra for bare β-Ga_2O_3 substrate and 100 nm SiO_2 covered β-Ga_2O_3 is shown in Fig. 3A and B respectively. The data was taken using 532 nm laser. The data taken with 473 and 660 nm lasers are presented in Figs. S1 and S2 respectively. The common peaks in β-Ga_2O_3 are marked in the figure. The peak positions of the different modes for both samples are listed in Table 1 along with their full width at half maximum (FWHM). The peak positions have been determined by fitting a Lorentz function to the Raman data [65]. While the bare substrate data fits well with the Lorentzian peak fit, some peaks in SiO_2 covered substrate are best fitted with Voigt function. The results of the peak fitting using Voigt function are shown in Table S1. The FWHM of the peaks fitted with Voigt function have been calculated on the basis of definition given by Olivero et al. [66]. GLmix in the table (Table S1) defines the proportion of Lorentzian character of the Voigt function [67]. The relative intensities (Rel. Int.) of the peaks are calculated from the area of the fitted curves and has been normalised with respect to A3 peak. The peaks of B3 and B4 modes are very close to A5 and A7 respectively and is indistinguishable from each other. Hence, the modes A5, B3 and A7, B4 are represented together in the table. The relative intensities on β-Ga_2O_3 show trends similar to that shown by Kranert et al. [65] In contrast, there is considerable deviation in the intensity trends for SiO_2 covered β-Ga_2O_3 and follows more closely the intensity trend of parallel polarisation along the [102] direction on $(\bar{2}01)$ β-Ga_2O_3.

The peaks in the data can be divided into three distinct regions [64]. First region are the peaks below 200 cm^{-1}, the second region are the peaks between 300 and 500 cm^{-1} and the third one are the peaks above 600 cm^{-1}. The peaks below 200 cm^{-1} are associated with vibrations of the tetrahedra chains [64] i.e. small amplitudes and have narrow widths of ~3 cm^{-1}. In this region the FWHM of the peaks are slightly wider for SiO_2 covered β-Ga_2O_3 and this trend is seen for most peaks. The intensity trend is similar except for the B1 and B2 modes having lower intensities. However, the intensity trend for the peaks beyond 200 cm^{-1} is completely different for β-Ga_2O_3 and SiO_2 covered β-Ga_2O_3. In this region the peaks are broader (FWHM > 3 cm^{-1}). The modes above 200 cm^{-1} correspond to bending and stretching modes or internal vibrations of the tetrahedra groups. The presence of the SiO_2 layer on top of β-Ga_2O_3 seem to have disproportionate effect on these modes. Finally, Raman spectra of diamond film grown on SiO_2 covered β-Ga_2O_3 has been taken and the data is presented in Fig. 4. The data was taken with 532 nm laser. The spectra from β-Ga_2O_3, SiO_2 coated β-Ga_2O_3 and diamond taken with 532 nm laser are presented together in Fig. S3 for comparison.

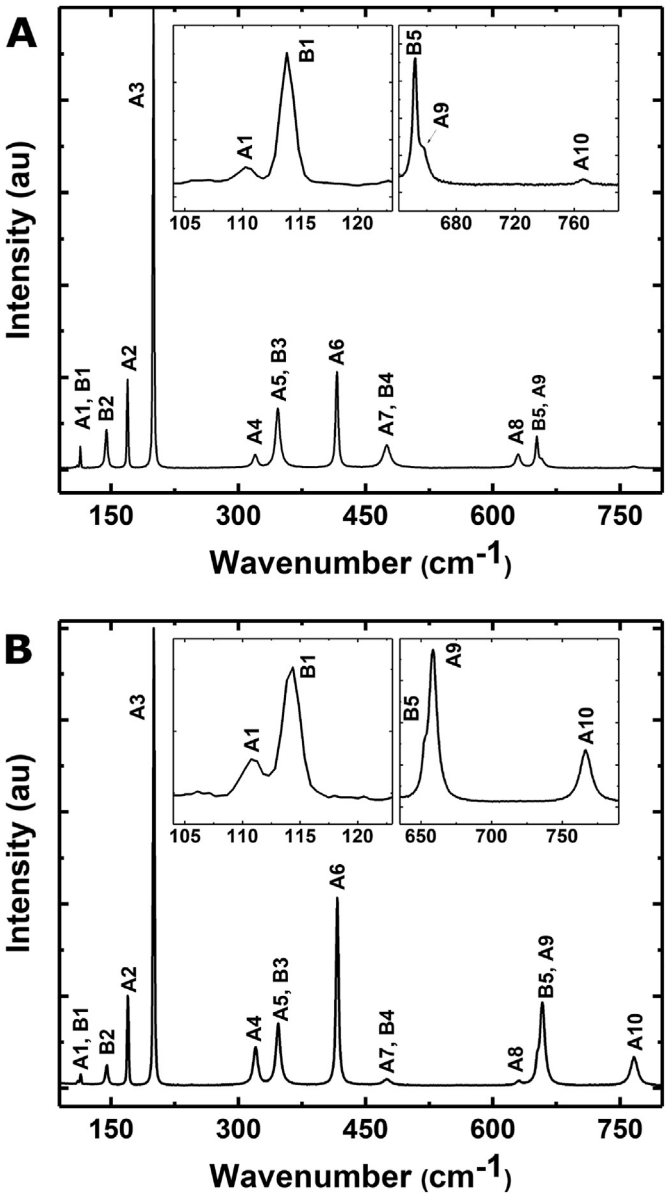

Fig. 3. Raman spectroscopy data is shown for A) β-Ga_2O_3 and B) SiO_2 covered β-Ga_2O_3. The common peaks are marked in the figure. The inset shows the magnified view of A1, B1 peaks (left inset) and B5, A9 and A10 peaks (right inset). Note the change in relative intensities of various peaks in bare substrate and SiO_2 covered substrate, specifically A6, B5, A9 and A10. The data was taken using 532 nm laser.

The Raman spectroscopy data for diamond thin film on SiO_2 coated β-Ga_2O_3, shown in Fig. 4A, shows a clear diamond peak. The data was taken with 532 nm excitation laser and a straight line luminescence background was subtracted [68] before presenting the data in the figure. Data was also taken with 473 and 660 nm excitation. The data taken at 473 nm also showed luminescence background, however the background was absent for the data taken at 660 nm [69]. The β-Ga_2O_3 Raman peaks were present in all three dataset and the same are shown in Fig. S4. The figure also shows the background straight line subtracted for the data in Fig. 4. The commonly observed peaks in thin diamond films are marked in Fig. 4. The small shoulder around 1350 cm^{-1} is associated with the D peak from amorphous carbon [70–72]. The peak at around

Table 1
Peak positions, FWHM and relative intensity with respect to A3 of Raman peaks for β-Ga_2O_3 and SiO_2 coated β-Ga_2O_3. The peak positions and FWHM are in cm^{-1}.

Raman mode	β-Ga_2O_3			SiO_2 on β-Ga_2O_3		
	Peak Center	FWHM	Rel. Int.	Peak Center	FWHM	Rel. Int.
A1	109.95	2.30	8.70	110.67	2.27	7.66
B1	113.89	1.31	35.29	114.24	1.68	19.67
B2	144.54	3.15	144.97	144.93	3.39	72.91
A2	169.44	1.67	189.92	169.84	1.84	195.13
A3	199.99	1.70	1000	200.41	1.90	1000
A4	319.85	5.69	83.19	320.36	5.94	241.01
A5, B3	346.56	6.03	419.67	347.00	6.06	398.24
A6	416.28	3.27	378.74	416.75	3.39	701.80
A7, B4	475.03	9.76	256.77	475.15	10.28	62.19
A8	629.77	6.46	101.68	630.59	7.02	28.81
B5	651.88	3.49	121.95	652.34	3.47	54.73
A9	658.04	6.61	51.97	658.50	6.78	604.38
A10	766.20	8.43	13.70	766.53	9.69	295.99

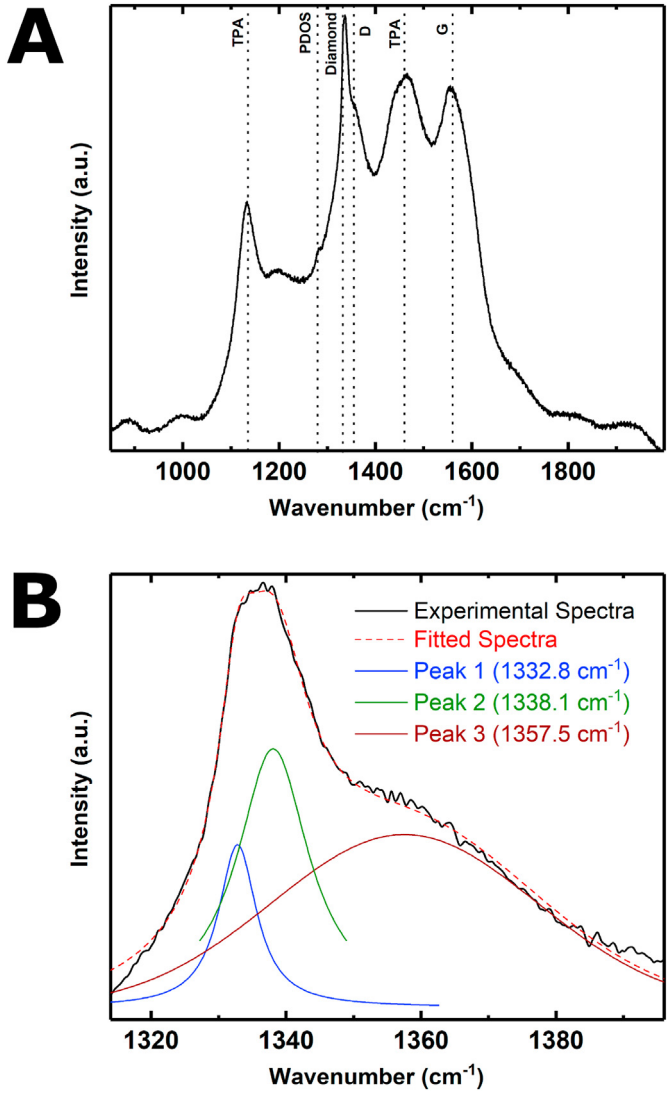

Fig. 4. A. Raman spectroscopy data is shown for diamond thin film grown on SiO_2 coated β-Ga_2O_3. The positions of common Raman peaks seen in diamond thin films are marked in the figure. The data was taken using 532 nm laser. B. The zoomed in view of the diamond peak is shown along with the fitted curves. The peak has been fitted with two Lorentzian and one Gaussian curve. (A colour version of this figure can be viewed online.)

1332 cm^{-1} is the diamond peak [73,74], however, it is clearly shifted towards higher wavenumbers and is heavily convoluted with additional bands. This is likely due to stress in the diamond thin film [75–79]. Accurate determination of the stress magnitude requires appropriate deconvolution of the spectra. Gries et al. [80] demonstrated that multiple types were required to resolve the spectra; 1 Gaussian for non-diamond carbon and 3 Lorentzians for diamond peaks in various stress states. In the simplest way, resolving the spectra between 1300 and 1400 cm^{-1} for one Lorentzian and one Gaussian profiles yield peak positions of 1336 cm^{-1} and 1359.4 cm^{-1} for the diamond and D peaks, respectively. The FWHM of the two fitted peaks were 14.9 and 53.2 cm^{-1} respectively. In a similar approach to Gries et al. [80], the spectra in this work obtained a better fit (higher R^2 and lower χ^2) using 2 Lorentzian peaks to resolve the diamond contributions (1332.8 and 1338.1 cm^{-1}) and a Gaussian peak to resolve the D peak (1357.5 cm^{-1}). The FWHM of the diamond peaks as determined by the fits are 6.8 and 12.8 cm^{-1} respectively. The FWHM of the D peak is 46.2 cm^{-1}. Further increment in number of peaks results in non-convergence of the fitting parameters and leads to unfeasible results. Fig. 4B shows the zoomed view of the diamond peak and D peak from amorphous carbon. The deconvoluted peaks along with the calculated curve are shown in the figure.

Considering the fits to the diamond peak in Fig. 4B the shift in the peak is between 4 and 6 cm^{-1}, depending on whether one considers the resolved or unresolved peak. Various researchers have estimated different stress coefficients for Raman peak shifts. Boppart et al. [81] estimated the stress coefficient for Raman line shifts to be around 0.38 GPa/cm^{-1} by measuring the shifts in Raman line for a diamond crystal under pressure. Knight et al. [75] and Ager [82] concluded a similar coefficient of 0.42 GPa/cm^{-1} and 0.49 GPa/cm^{-1}, respectively, by measuring stress in diamond films. However, Yoshikawa et al. [83,84] used the value of 2.63 GPa/cm^{-1} for their results assuming only hydrostatic stress. Windischmann et al. [77] used a value of 0.39 GPa/cm^{-1}, however the postulated that films grown on substrates are under biaxial stress, hence the coefficient is 1.5 times larger resulting in a coefficient of 0.59 GPa/cm^{-1}. These figures were later disputed by Anastassakis [78]. Based on equations given by Anastasskis [78], the stress in the diamond films presented in this work is estimated to be between 1.3 and 2.8 GPa (assuming bisotropic stress), which is closer to the results of Boppart et al. [81] and Knight et al. [75]. The stress along with adhesion strength between various components of the stack consisting of β-Ga_2O_3, SiO_2 and diamond will determine if a film will stick on the substrate. It should be noted that the stress between layers is thickness dependent [85]. In the case of diamond on SiO_2 covered β-Ga_2O_3 the film thickness is limited to 250 nm.

Fig. 4A also shows peaks at ~1150 and ~1450 cm^{-1}. These are associated with the transpolyacetylene present at grain boundaries and diamond surface [86]. The peak around ~1560 cm^{-1} is associated with G peak from amorphous carbon [71,72]. Apart from these a small shoulder can be seen around ~1280 cm^{-1}. This is associated with phonon density of states (PDOS) in diamond [71,87]. Small bumps around 900, 1000 and 1220 cm^{-1} can also be seen which can also be attributed to PDOS of diamond [87].

4. Conclusion

In conclusion, the ζ-potential of β-Ga_2O_3 has been presented. The ζ-potential was found to be negative above pH ~ 4.6, enabling the use of H-terminated diamond seed solution for seeding of the surface. The ζ-potential is similar to that of Ga-faced gallium nitride. In contrast gallium oxide nanoparticles have largely

positive ζ-potential with isoelectric poit at pH∼9 [59] A method for growing diamond on β-Ga_2O_3 crystal has also been detailed. It was found that direct growth of diamond on β-Ga_2O_3 is not possible with MPCVD. As a result, thin layer of Al_2O_3 and SiO_2 were deposited on β-Ga_2O_3 before diamond deposition. Upon seeding with diamond solution, SiO_2 layer survived the diamond growth condition and resulted in a thin diamond layer. In contrast the seeded Al_2O_3 layer of similar thickness was completely destroyed when exposed to diamond growth conditions. Raman measurements were done on β-Ga_2O_3, coated β-Ga_2O_3 and diamond on coated β-Ga_2O_3. It was found that the diamond layer is under considerable amount of stress and this is due to the mismatch in thermal expansion coefficient between β-Ga_2O_3 and diamond. Further work is needed to manage the interfacial stress between diamond and coated β-Ga_2O_3 for growth of thick diamond layer on β-Ga_2O_3.

CRediT authorship contribution statement

Soumen Mandal: Conceptualization, Methodology, Formal analysis, Investigation, Resources, Writing – original draft, Writing – review & editing, Project administration. **Karsten Arts:** Resources, Writing – original draft, Writing – review & editing. **Harm C.M. Knoops:** Resources, Writing – review & editing. **Jerome A. Cuenca:** Investigation, Writing – review & editing. **Georgina M. Klemencic:** Investigation, Writing – review & editing. **Oliver A. Williams:** Conceptualization, Methodology, Writing – review & editing, Project administration, Funding acquisition.

Declaration of competing interest

The authors declare that they have no known competing financial interests or personal relationships that could have appeared to influence the work reported in this paper.

Acknowledgment

This project has been supported by Engineering and Physical Sciences Research Council under programme Grant GaN-DaME (EP/P00945X/1). The metadata for the results presented in this paper can be found in https://doi.org/10.17035/d.2021.0134023831.

Appendix A. Supplementary data

Supplementary data to this article can be found online at https://doi.org/10.1016/j.carbon.2021.04.100.

References

[1] J. Casady, R. Johnson, Status of silicon carbide (SiC) as a wide-bandgap semiconductor for high-temperature applications: a review, Solid State Electron. 39 (10) (1996) 1409–1422, https://doi.org/10.1016/0038-1101(96)00045-7, 10.1016/0038-1101(96)00045-7.

[2] U. Mishra, Likun Shen, T. Kazior, Yi-Feng Wu, GaN-based RF power devices and amplifiers, Proc. IEEE 96 (2) (2008) 287–305, https://doi.org/10.1109/JPROC.2007.911060, 10.1109/JPROC.2007.911060.

[3] B.J. Baliga, Semiconductors for high–voltage, vertical channel field–effect transistors, J. Appl. Phys. 53 (3) (1982) 1759–1764, https://doi.org/10.1063/1.331646, 10.1063/1.331646.

[4] E.O. Johnson, Physical limitations on frequency and power parameters of transistors, RCA Rev. 26 (1965) 163–177.

[5] J.Y. Tsao, S. Chowdhury, M.A. Hollis, D. Jena, N.M. Johnson, K.A. Jones, R.J. Kaplar, S. Rajan, C.G. Van de Walle, E. Bellotti, C.L. Chua, R. Collazo, M.E. Coltrin, J.A. Cooper, K.R. Evans, S. Graham, T.A. Grotjohn, E.R. Heller, M. Higashiwaki, M.S. Islam, P.W. Juodawlkis, M.A. Khan, A.D. Koehler, J.H. Leach, U.K. Mishra, R.J. Nemanich, R.C.N. Pilawa-Podgurski, J.B. Shealy, Z. Sitar, M.J. Tadjer, A.F. Witulski, M. Wraback, J.A. Simmons, Ultrawide-bandgap semiconductors: Research opportunities and challenges, Adv. Electr. Mater. 4 (1) (2018), https://doi.org/10.1002/aelm.201600501, 1600501. doi:10.1002/aelm.201600501.

[6] M. Higashiwaki, K. Sasaki, H. Murakami, Y. Kumagai, A. Koukitu, A. Kuramata, T. Masui, S. Yamakoshi, Recent progress in Ga 2 O 3 power devices, Semicond. Sci. Technol. 31 (3) (2016), https://doi.org/10.1088/0268-1242/31/3/034001, 034001. doi:10.1088/0268-1242/31/3/034001.

[7] S.J. Pearton, F. Ren, M. Tadjer, J. Kim, Perspective: Ga^2O^3 for ultra-high power rectifiers and MOSFETS, J. Appl. Phys. 124 (22) (2018), https://doi.org/10.1063/1.5062841, 220901. doi:10.1063/1.5062841.

[8] S.J. Pearton, J. Yang, P.H. Cary, F. Ren, J. Kim, M.J. Tadjer, M.A. Mastro, A review of Ga 2 O 3 materials, processing, and devices, Appl. Phys. Rev. 5 (1) (2018), https://doi.org/10.1063/1.5006941, 011301. doi:10.1063/1.5006941.

[9] M. Higashiwaki, G.H. Jessen, Guest Editorial: the dawn of gallium oxide microelectronics, Appl. Phys. Lett. 112 (6) (2018), https://doi.org/10.1063/1.5017845, 060401. doi:10.1063/1.5017845.

[10] H.W. Xue, Q.M. He, G.Z. Jian, S.B. Long, T. Pang, M. Liu, An overview of the ultrawide bandgap Ga^2O^3 semiconductor-based Schottky barrier diode for power electronics application, Nanoscale Res. Lett. 13 (2018) 290, https://doi.org/10.1186/s11671-018-2712-1, 10.1186/s11671-018-2712-1.

[11] E.G. Víllora, K. Shimamura, Y. Yoshikawa, K. Aoki, N. Ichinose, Large-size ^{β}-Ga2O3 single crystals and wafers, J. Cryst. Growth 270 (3–4) (2004) 420–426, https://doi.org/10.1016/j.jcrysgro.2004.06.027, 10.1016/j.jcrysgro.2004.06.027.

[12] S. Ohira, M. Yoshioka, T. Sugawara, K. Nakajima, T. Shishido, Fabrication of hexagonal GaN on the surface of ^{β}-Ga2O3 single crystal by nitridation with NH3, Thin Solid Films 496 (1) (2006) 53–57, https://doi.org/10.1016/j.tsf.2005.08.230, 10.1016/j.tsf.2005.08.230.

[13] Y. Tomm, P. Reiche, D. Klimm, T. Fukuda, Czochralski grown Ga2O3 crystals, J. Cryst. Growth 220 (4) (2000) 510–514, https://doi.org/10.1016/S0022-0248(00)00851-4, 10.1016/S0022-0248(00)00851-4.

[14] Z. Galazka, R. Uecker, D. Klimm, K. Irmscher, M. Naumann, M. Pietsch, A. Kwasniewski, R. Bertram, S. Ganschow, M. Bickermann, Scaling-up of bulk ^{β}-Ga 2 O 3 single crystals by the Czochralski method, ECS J. Solid State Sci. Technol. 6 (2) (2017) Q3007–Q3011, https://doi.org/10.1149/2.0021702jss, 10.1149/2.0021702jss.

[15] K. Hoshikawa, E. Ohba, T. Kobayashi, J. Yanagisawa, C. Miyagawa, Y. Nakamura, Growth of ^{β}-Ga2O3 single crystals using vertical Bridgman method in ambient air, J. Cryst. Growth 447 (2016) 36–41, https://doi.org/10.1016/j.jcrysgro.2016.04.022, 10.1016/j.jcrysgro.2016.04.022.

[16] E. Ohba, T. Kobayashi, M. Kado, K. Hoshikawa, Defect characterization of ^{β}-Ga 2 O 3 single crystals grown by vertical Bridgman method, Jpn. J. Appl. Phys. 55 (12) (2016), https://doi.org/10.7567/JJAP.55.1202BF, 1202BF. doi:10.7567/JJAP.55.1202BF.

[17] H. Aida, K. Nishiguchi, H. Takeda, N. Aota, K. Sunakawa, Y. Yaguchi, Growth of ^{β}-Ga 2 O 3 single crystals by the edge-defined, film fed growth method, Jpn. J. Appl. Phys. 47 (11) (2008) 8506–8509, https://doi.org/10.1143/JJAP.47.8506, 10.1143/JJAP.47.8506.

[18] A. Kuramata, K. Koshi, S. Watanabe, Y. Yamaoka, T. Masui, S. Yamakoshi, High-quality ^{β}-Ga 2 O 3 single crystals grown by edge-defined film-fed growth, Jpn. J. Appl. Phys. 55 (12) (2016), https://doi.org/10.7567/JJAP.55.1202A2, 1202A2. doi:10.7567/JJAP.55.1202A2.

[19] M. Higashiwaki, K. Sasaki, A. Kuramata, T. Masui, S. Yamakoshi, Gallium oxide (Ga 2 O 3) metal-semiconductor field-effect transistors on single-crystal ^{β}-Ga 2 O 3 (010) substrates, Appl. Phys. Lett. 100 (1) (2012), https://doi.org/10.1063/1.3674287, 013504. doi:10.1063/1.3674287.

[20] M. Higashiwaki, K. Sasaki, T. Kamimura, M. Hoi Wong, D. Krishnamurthy, A. Kuramata, T. Masui, S. Yamakoshi, Depletion-mode Ga 2 O 3 metal-oxide-semiconductor field-effect transistors on ^{β}-Ga 2 O 3 (010) substrates and temperature dependence of their device characteristics, Appl. Phys. Lett. 103 (12) (2013), https://doi.org/10.1063/1.4821858, 123511. doi:10.1063/1.4821858.

[21] K.D. Chabak, N. Moser, A.J. Green, D.E. Walker, S.E. Tetlak, E. Heller, A. Crespo, R. Fitch, J.P. McCandless, K. Leedy, M. Baldini, G. Wagner, Z. Galazka, X. Li, G. Jessen, Enhancement-mode Ga 2 O 3 wrap-gate fin field-effect transistors on native (100) ^{β}-Ga 2 O 3 substrate with high breakdown voltage, Appl. Phys. Lett. 109 (21) (2016), https://doi.org/10.1063/1.4967931, 213501. doi:10.1063/1.4967931.

[22] A.J. Green, K.D. Chabak, E.R. Heller, R.C. Fitch, M. Baldini, A. Fiedler, K. Irmscher, G. Wagner, Z. Galazka, S.E. Tetlak, A. Crespo, K. Leedy, G.H. Jessen, 3.8-MV/cm breakdown strength of MOVPE-grown Sn-doped ^{β}-Ga2O3 MOSFETs, IEEE Electron. Device Lett. 37 (7) (2016) 902–905, https://doi.org/10.1109/LED.2016.2568139, 10.1109/LED.2016.2568139.

[23] M.H. Wong, K. Sasaki, A. Kuramata, S. Yamakoshi, M. Higashiwaki, Field-plated Ga 2 O 3 MOSFETs with a breakdown voltage of over 750 V, IEEE Electron. Device Lett. 37 (2) (2016) 212–215, https://doi.org/10.1109/LED.2015.2512279, 10.1109/LED.2015.2512279.

[24] N.A. Moser, J.P. McCandless, A. Crespo, K.D. Leedy, A.J. Green, E.R. Heller, K.D. Chabak, N. Peixoto, G.H. Jessen, High pulsed current density ^{β}-Ga2O3 MOSFETs verified by an analytical model corrected for interface charge, Appl. Phys. Lett. 110 (14) (2017), https://doi.org/10.1063/1.4979789, 143505. doi:10.1063/1.4979789.

[25] H. Zhou, K. Maize, G. Qiu, A. Shakouri, P.D. Ye, ^{β}-Ga2O3 on insulator field-effect transistors with drain currents exceeding 1.5 A/mm and their self-heating effect, Appl. Phys. Lett. 111 (9) (2017), https://doi.org/10.1063/1.5000735, 092102. doi:10.1063/1.5000735.

[26] J. Noh, P.D. Ye, S. Alajlouni, M.J. Tadjer, J.C. Culbertson, H. Bae, M. Si, H. Zhou, P.A. Bermel, A. Shakouri, High performance ^{β}-Ga2O3 nano-membrane field

effect transistors on a high thermal conductivity diamond substrate, IEEE J. Electron Devices Soc. 7 (June) (2019) 914–918, https://doi.org/10.1109/JEDS.2019.2933369, 10.1109/JEDS.2019.2933369.
[27] H. Kim, S. Tarelkin, A. Polyakov, S. Troschiev, S. Nosukhin, M. Kuznetsov, J. Kim, Ultrawide-bandgap p-n heterojunction of diamond/β-Ga2O3 for a solar-blind photodiode, ECS J. Solid State Sci. Technol. 9 (4) (2020), https://doi.org/10.1149/2162-8777/ab89b8, 045004. doi:10.1149/2162-8777/ab89b8.
[28] Z. Guo, A. Verma, X. Wu, F. Sun, A. Hickman, T. Masui, A. Kuramata, M. Higashiwaki, D. Jena, T. Luo, Anisotropic thermal conductivity in single crystal β-gallium oxide, Appl. Phys. Lett. 106 (11) (2015) 1–6, https://doi.org/10.1063/1.4916078, 10.1063/1.4916078.
[29] Sangmin Lee, R. Vetury, J.D. Brown, S.R. Gibb, W.Z. Cai, Jinming Sun, D.S. Green, J. Shealy, Reliability assessment of AlGaN/GaN HEMT technology on SiC for 48V applications, in: IEEE International Reliability Physics Symposium, IEEE, 2008, pp. 446–449, https://doi.org/10.1109/RELPHY.2008.4558926, 10.1109/RELPHY.2008.4558926.
[30] J.W. Pomeroy, M.J. Uren, B. Lambert, M. Kuball, Operating channel temperature in GaN HEMTs: DC versus RF accelerated life testing, Microelectron. Reliab. 55 (12) (2015) 2505–2510, https://doi.org/10.1016/j.microrel.2015.09.025, 10.1016/j.microrel.2015.09.025.
[31] Z. Cheng, L. Yates, J. Shi, M.J. Tadjer, K.D. Hobart, S. Graham, Thermal conductance across β-Ga 2 O 3 -diamond van der Waals heterogeneous interfaces, Apl. Mater. 7 (3) (2019), https://doi.org/10.1063/1.5089559, 031118. doi:10.1063/1.5089559.
[32] Z. Cheng, V.D. Wheeler, T. Bai, J. Shi, M.J. Tadjer, T. Feygelson, K.D. Hobart, M.S. Goorsky, S. Graham, Integration of polycrystalline Ga 2 O 3 on diamond for thermal management, Appl. Phys. Lett. 116 (6) (2020), https://doi.org/10.1063/1.5125637, 062105. doi:10.1063/1.5125637.
[33] T. Matsumae, Y. Kurashima, H. Umezawa, K. Tanaka, T. Ito, H. Watanabe, H. Takagi, Low-temperature direct bonding of β-Ga 2 O 3 and diamond substrates under atmospheric conditions, Appl. Phys. Lett. 116 (14) (2020), https://doi.org/10.1063/5.0002068, 141602. doi:10.1063/5.0002068.
[34] M. Schreck, S. Gsell, R. Brescia, M. Fischer, Ion bombardment induced buried lateral growth: the key mechanism for the synthesis of single crystal diamond wafers, Sci. Rep. 7 (1) (2017), https://doi.org/10.1038/srep44462, 44462. doi:10.1038/srep.44462.
[35] E.L. Thomas, G.W. Nelson, S. Mandal, J.S. Foord, O.a. Williams, Chemical mechanical polishing of thin film diamond, Carbon 68 (2014) 473–479, https://doi.org/10.1016/j.carbon.2013.11.023, 10.1016/j.carbon.2013.11.023.
[36] J.M. Werrell, S. Mandal, E.L.H. Thomas, E.B. Brousseau, R. Lewis, P. Borri, P.R. Davies, O.A. Williams, Effect of slurry composition on the chemical mechanical polishing of thin diamond films, Sci. Technol. Adv. Mater. 18 (1) (2017) 654–663, https://doi.org/10.1080/14686996.2017.1366815, 10.1080/14686996.2017.1366815.
[37] S. Mandal, E.L. Thomas, L. Gines, D. Morgan, J. Green, E.B. Brousseau, O.A. Williams, Redox agent enhanced chemical mechanical polishing of thin film diamond, Carbon 130 (2018) 25–30, https://doi.org/10.1016/j.carbon.2017.12.077, 10.1016/j.carbon.2017.12.077.
[38] S. Mandal, C. Yuan, F. Massabuau, J.W. Pomeroy, J. Cuenca, H. Bland, E. Thomas, D. Wallis, T. Batten, D. Morgan, R. Oliver, M. Kuball, O.A. Williams, Thick, adherent diamond films on AlN with low thermal barrier resistance, ACS Appl. Mater. Interfaces 11 (43) (2019) 40826–40834, https://doi.org/10.1021/acsami.9b13869, 10.1021/acsami.9b13869.
[39] W.D. Harkins, Energy relations of the surface of solids I. Surface energy of the diamond, J. Chem. Phys. 10 (5) (1942) 268–272, https://doi.org/10.1063/1.1723719, 10.1063/1.1723719.
[40] R.J. Jaccodine, Surface energy of germanium and silicon, J. Electrochem. Soc. 110 (6) (1963) 524, https://doi.org/10.1149/1.2425806, 10.1149/1.2425806.
[41] O. Williams, Nanocrystalline diamond, Diam. Relat. Mater. 20 (5–6) (2011) 621–640, https://doi.org/10.1016/j.diamond.2011.02.015, 10.1016/j.diamond.2011.02.015.
[42] S. Mandal, Nucleation of diamond films on heterogeneous substrates: a review, RSC Adv. 11 (2021) 10159–10182, https://doi.org/10.1039/D1RA00397F, 10.1039/D1RA00397F.
[43] V. Bermudez, The structure of low-index surfaces of β-Ga2O3, Chem. Phys. 323 (2–3) (2006) 193–203, https://doi.org/10.1016/j.chemphys.2005.08.051, 10.1016/j.chemphys.2005.08.051.
[44] A.Y. Polyakov, I.-H. Lee, N.B. Smirnov, E.B. Yakimov, I.V. Shchemerov, A.V. Chernykh, A.I. Kochkova, A.A. Vasilev, F. Ren, P.H. Carey, S.J. Pearton, Hydrogen plasma treatment of β-Ga 2 O 3: changes in electrical properties and deep trap spectra, Appl. Phys. Lett. 115 (3) (2019), 032101. doi:10.1063/1.5108790, http://aip.scitation.org/doi/10.1063/1.5108790.
[45] R. Van Wagenen, J. Andrade, Flat plate streaming potential investigations: hydrodynamics and electrokinetic equivalency, J. Colloid Interface Sci. 76 (2) (1980) 305–314, https://doi.org/10.1016/0021-9797(80)90374-4, 10.1016/0021-9797(80)90374-4.
[46] A. Voigt, H. Wolf, S. Lauekner, G. Neumann, R. Becker, L. Richter, Electrokinetic properties of polymer and glass surfaces in aqueous solutions: experimental evidence for swollen surface layers, Biomaterials 4 (4) (1983) 299–304, 10.1016/0142-9612(83)90032-7, http://linkinghub.elsevier.com/retrieve/pii/0142961283900327.
[47] W. Norde, E. Rouwendal, Streaming potential measurements as a tool to study protein adsorption kinetics, J. Colloid Interface Sci. 139 (1) (1990) 169–176, 10.1016/0021-9797(90)90454-V, http://linkinghub.elsevier.com/retrieve/pii/002197979090454V.
[48] P.J. Scales, F. Grieser, T.W. Healy, Electrokinetics of the muscovite mica-aqueous solution interface, Langmuir 6 (3) (1990) 582–589, 10.1021/la00093a012, http://pubs.acs.org/doi/abs/10.1021/la00093a012.
[49] S. Mandal, E.L.H. Thomas, C. Middleton, L. Gines, J.T. Griffiths, M.J. Kappers, R.A. Oliver, D.J. Wallis, L.E. Goff, S.A. Lynch, M. Kuball, O.A. Williams, Surface zeta potential and diamond seeding on gallium nitride films, ACS Omega 2 (10) (2017) 7275–7280, arXiv:1707.05410, doi:10.1021/acsomega.7b01069, http://pubs.acs.org/doi/10.1021/acsomega.7b01069.
[50] H.A. Bland, E.L.H. Thomas, G.M. Klemencic, S. Mandal, D.J. Morgan, A. Papageorgiou, T.G. Jones, O.A. Williams, Superconducting diamond on silicon nitride for device applications, Sci. Rep. 9 (1) (2019) 2911, https://doi.org/10.1038/s41598-019-39707-z, 10.1038/s41598-019-39707-z.
[51] S. Mandal, H.A. Bland, J.A. Cuenca, M. Snowball, O. Williams, Superconducting boron doped nanocrystalline diamond on boron nitride ceramics, Nanoscale 11 (2019), https://doi.org/10.1039/C9NR02729G, 10266. doi:10.1039/C9NR02729G.
[52] H.A. Bland, I.A. Centeleghe, S. Mandal, E.L.H. Thomas, J.-y. Maillard, O.A. Williams, Electropositive nanodiamond-coated quartz microfiber membranes for virus and dye filtration, ACS Appl. Nano Mater. 4 (3) (2021) 3252–3261, 10.1021/acsanm.1c00439, https://pubs.acs.org/doi/10.1021/acsanm.1c00439.
[53] C. Werner, H. Körber, R. Zimmermann, S. Dukhin, H.-J. Jacobasch, Extended electrokinetic characterization of flat solid surfaces, J. Colloid Interface Sci. 208 (1) (1998) 329–346, 10.1006/jcis.1998.5787, http://linkinghub.elsevier.com/retrieve/pii/S0021979798957873.
[54] S.B.S. Heil, J.L. van Hemmen, C.J. Hodson, N. Singh, J.H. Klootwijk, F. Roozeboom, M.C.M. van de Sanden, W.M.M. Kessels, Deposition of TiN and HfO[sub 2] in a commercial 200 mm remote plasma atomic layer deposition reactor, J. Vac. Sci. Technol.: Vacuum Surf. Films 25 (5) (2007) 1357, 10.1116/1.2753846, http://scitation.aip.org/content/avs/journal/jvsta/25/5/10.1116/1.2753846.
[55] E. Langereis, S.B.S. Heil, H.C.M. Knoops, W. Keuning, M.C.M. van de Sanden, W.M.M. Kessels, In situ spectroscopic ellipsometry as a versatile tool for studying atomic layer deposition, J. Phys. Appl. Phys. 42 (7) (2009), 073001. doi:10.1088/0022-3727/42/7/073001, https://iopscience.iop.org/article/10.1088/0022-3727/42/7/073001.
[56] C. Moelle, S. Klose, F. Szücs, H. Fecht, C. Johnston, P. Chalker, M. Werner, Measurement and calculation of the thermal expansion coefficient of diamond, Diam. Relat. Mater. 6 (5–7) (1997) 839–842, 10.1016/S0925-9635(96)00674-7, https://linkinghub.elsevier.com/retrieve/pii/S0925963596006747.
[57] Z. Cheng, M. Hanke, Z. Galazka, A. Trampert, Thermal expansion of single-crystalline β-Ga 2 O 3 from RT to 1200 K studied by synchrotron-based high resolution x-ray diffraction, Appl. Phys. Lett. 113 (18) (2018), https://doi.org/10.1063/1.5054265, 182102. doi:10.1063/1.5054265, https://aip.scitation.org/doi/10.1063/1.5054265.
[58] J. Hees, A. Kriele, O.A. Williams, Electrostatic self-assembly of diamond nanoparticles, Chem. Phys. Lett. 509 (1–3) (2011) 12–15, https://doi.org/10.1016/j.cplett.2011.04.083, 10.1016/j.cplett.2011.04.083.
[59] M. Kosmulski, Pristine points of zero charge of gallium and indium oxides, J. Colloid Interface Sci. 238 (1) (2001) 225–227, 10.1006/jcis.2001.7484, https://linkinghub.elsevier.com/retrieve/pii/S0021979701974843.
[60] G. Chen, Z. Ni, Y. Bai, Q. Li, Y. Zhao, The role of interactions between abrasive particles and the substrate surface in chemical-mechanical planarization of Si-face 6H-SiC, RSC Adv. 7 (28) (2017) 16938–16952, https://doi.org/10.1039/C6RA27508G, 10.1039/C6RA27508G.
[61] J.L. Reyes Bahena, A. Robledo Cabrera, A. López Valdivieso, R. Herrera Urbina, Fluoride adsorption onto α-Al 2 O 3 and its effect on the zeta potential at the alumina–aqueous electrolyte interface, Separ. Sci. Technol. 37 (8) (2002) 1973–1987, https://doi.org/10.1081/SS-120003055, 10.1081/SS-120003055.
[62] J.W. Lee, B. Pathangey, M.R. Davidson, P.H. Holloway, E.S. Lambers, B. Davydov, T.J. Anderson, S.J. Pearton, Comparison of plasma chemistries for dry etching thin film electroluminescent display materials, J. Vac. Sci. Technol.: Vacuum Surf. Films 16 (4) (1998) 2177–2186, 10.1116/1.581326, http://avs.scitation.org/doi/10.1116/1.581326.
[63] B. Lee, T.R. Hayes, P.M. Thomas, R. Pawelek, P.F. Sciortino, SiO 2 mask erosion and sidewall composition during CH 4/H 2 reactive ion etching of InGaAsP/InP, Appl. Phys. Lett. 63 (23) (1993) 3170–3172, 10.1063/1.110213, http://aip.scitation.org/doi/10.1063/1.110213.
[64] D. Dohy, G. Lucazeau, A. Revcolevschi, Raman spectra and valence force field of single-crystalline βGa2O3, J. Solid State Chem. 45 (2) (1982) 180–192, https://doi.org/10.1016/0022-4596(82)90274-2, 10.1016/0022-4596(82)90274-2.
[65] C. Kranert, C. Sturm, R. Schmidt-Grund, M. Grundmann, Raman tensor elements of β-Ga2O3, Sci. Rep. 6 (2016) 1–9, https://doi.org/10.1038/srep35964, 10.1038/srep.35964.
[66] J. Olivero, R. Longbothum, Empirical fits to the Voigt line width: a brief review, J. Quant. Spectrosc. Radiat. Transf. 17 (2) (1977) 233–236, https://doi.org/10.1016/0022-4073(77)90161-3, 10.1016/0022-4073(77)90161-3.
[67] P.M. Sherwood, Rapid evaluation of the Voigt function and its use for interpreting X-ray photoelectron spectroscopic data, Surf. Interface Anal. 51 (2) (2019) 254–274, https://doi.org/10.1002/sia.6577, 10.1002/sia.6577.
[68] A. Dychalska, K. Fabisiak, K. Paprocki, J. Makowiecki, A. Iskaliyeva, M. Szybowicz, A Raman spectroscopy study of the effect of thermal treatment on structural and photoluminescence properties of CVD diamond films, Mater. Des. 112 (2016) 320–327, https://doi.org/10.1016/j.matdes.2016.09.092,

10.1016/j.matdes.2016.09.092.
[69] P.W. May, J.A. Smith, K.N. Rosser, 785 nm Raman spectroscopy of CVD diamond films, MRS Online Proc. Libr. 1039 (1) (2007) 1502, https://doi.org/10.1557/PROC-1039-P15-02, 10.1557/PROC-1039-P15-02.
[70] A.C. Ferrari, J. Robertson, Resonant Raman spectroscopy of disordered, amorphous, and diamondlike carbon, Phys. Rev. B 64 (7) (2001), 075414. doi:10.1103/PhysRevB.64.075414, http://link.aps.org/doi/10.1103/PhysRevB.64.075414.
[71] A.C. Ferrari, J. Robertson, Raman spectroscopy of amorphous, nanostructured, diamond–like carbon, and nanodiamond, Philos. Trans. R. Soc. London, Ser. A: Math. Phys. Eng. Sci. 362 (1824) (2004) 2477–2512, https://doi.org/10.1098/rsta.2004.1452, 10.1098/rsta.2004.1452.
[72] S. Prawer, R.J. Nemanich, Raman spectroscopy of diamond and doped diamond, Philos. Trans. R. Soc. London, Ser. A: Math. Phys. Eng. Sci. 362 (1824) (2004) 2537–2565, https://doi.org/10.1098/rsta.2004.1451, 10.1098/rsta.2004.1451.
[73] C. Ramaswamy, Raman effect in diamond, Nature 125 (1930) 704, https://doi.org/10.1038/125704b0, 704. doi:10.1038/125704b0.
[74] S. Bhagavantam, Relation of Raman effect to crystal structure, Indian J. Phys. 5 (1930) 169. http://hdl.handle.net/10821/555.
[75] D.S. Knight, W.B. White, Characterization of diamond films by Raman spectroscopy, J. Mater. Res. 4 (2) (1989) 385–393, 10.1557/JMR.1989.0385, http://link.springer.com/10.1557/JMR.1989.0385.
[76] J.W. Ager, M.D. Drory, Quantitative measurement of residual biaxial stress by Raman spectroscopy in diamond grown on a Ti alloy by chemical vapor deposition, Phys. Rev. B 48 (4) (1993) 2601–2607, https://doi.org/10.1103/PhysRevB.48.2601, 10.1103/PhysRevB.48.2601.
[77] H. Windischmann, K. Gray, Stress measurement of CVD diamond films, Diam. Relat. Mater. 4 (5–6) (1995) 837–842, https://doi.org/10.1016/0925-9635(94)05327-8, 10.1016/0925-9635(94)05327-8.
[78] E. Anastassakis, Strain characterization of polycrystalline diamond and silicon systems, J. Appl. Phys. 86 (1) (1999) 249–258, https://doi.org/10.1063/1.370723, 10.1063/1.370723.
[79] A. Dychalska, K. Fabisiak, K. Paprocki, A. Dudkowiak, M. Szybowicz, Temperature dependence of stress in CVD diamond films studied by Raman spectroscopy, Mater. Sci. Poland 33 (3) (2015) 620–626, https://doi.org/10.1515/msp-2015-0064, 10.1515/msp-2015-0064.
[80] T. Gries, L. Vandenbulcke, P. Simon, A. Canizares, Stresses in textured and polycrystalline cubic films by Raman spectroscopy: application to diamond, J. Appl. Phys. 102 (8). doi:10.1063/1.2798940. URL https://doi.org/10.1063/1.2798940.
[81] H. Boppart, J. van Straaten, I.F. Silvera, Raman spectra of diamond at high pressures, Phys. Rev. B 32 (2) (1985) 1423–1425, 10.1103/PhysRevB.32.1423, https://link.aps.org/doi/10.1103/PhysRevB.32.1423.
[82] J.W. Ager, Residual stress in diamond and amorphous carbon films, MRS Proc. 383 (1995) 143, https://doi.org/10.1557/PROC-383-143, in: http://link.springer.com/10.1557/PROC-383-143.
[83] M. Yoshikawa, G. Katagiri, H. Ishida, A. Ishitani, M. Ono, K. Matsumura, Characterization of crystalline quality of diamond films by Raman spectroscopy, Appl. Phys. Lett. 55 (25) (1989) 2608–2610, 10.1063/1.101951, http://aip.scitation.org/doi/10.1063/1.101951.
[84] M. Yoshikawa, H. Ishida, A. Ishitani, S. Koizumi, T. Inuzuka, Study of crystallographic orientations in the diamond film on the (100) surface of cubic boron nitride using a Raman microprobe, Appl. Phys. Lett. 58 (13) (1991) 1387–1388, https://doi.org/10.1063/1.104316, 10.1063/1.104316.
[85] J.A. Cuenca, M.D. Smith, D.E. Field, F.C.-P. Massabuau, S. Mandal, J. Pomeroy, D.J. Wallis, R.A. Oliver, I. Thayne, M. Kuball, O.A. Williams, Thermal stress modelling of diamond on GaN/III-Nitride membranes, Carbon 174 (2021) 647–661, https://doi.org/10.1016/j.carbon.2020.11.067, 10.1016/j.carbon.2020.11.067.
[86] A.C. Ferrari, J. Robertson, Origin of the 1150 cm $^{-1}$ Raman mode in nanocrystalline diamond, Phys. Rev. B 63 (12) (2001), 121405. doi:10.1103/PhysRevB.63.121405, https://link.aps.org/doi/10.1103/PhysRevB.63.121405.
[87] P. Pavone, K. Karch, O. Schütt, D. Strauch, W. Windl, P. Giannozzi, S. Baroni, Ab initio lattice dynamics of diamond, Phys. Rev. B 48 (5) (1993) 3156–3163, 10.1103/PhysRevB.48.3156, https://link.aps.org/doi/10.1103/PhysRevB.48.3156.